XFEM-BASED GEOMECHANICAL MODELLING OF POROUS MEDIA AT SMALL SCALE

B. Sonon, B. François, T.J. Massart
Building, Architecture & Town Planning CP 194/2, Université Libre de Bruxelles (ULB), Av. F.D. Roosevelt 50, 1050 Brussels, Belgium

ABSTRACT: *The numerical characterization of the geomechanical behaviour of geomaterials (soils, rocks or concrete) at small scale requires the consideration of the complex 3D geometries of their microstructures. It implies (i) difficulties to generate complex 3D Representative Volume Elements (RVEs), and (ii) major problems to discretize properly such RVEs to solve mechanical problems. We present here an integrated framework allowing morphological studies thanks to an efficient RVE generator coupled with an XFEM setting for three-dimensional mechanical simulations. Based on level set functions and "controlled" Random Sequential Packing algorithms, a dedicated tool for the generation of RVEs has been developed. The efficiency of the method is maximized by constraining the sequential addition process with a global level set function. The obtained RVEs respect the microstructural characteristics of the materials (grain size distribution, proportions of phases…). This microstructure generation tool is illustrated by the generation of 3D RVEs corresponding to various heterogeneous geomaterials. The microstructure is then discretized using a regular mesh using level set-based extended finite element (XFEM) approaches, which allow uncoupling the meshing operations from the presence of the (complex) fine scale material interfaces. Finally, fine scale constitutive laws, including plasticity, are used in computational homogenisation procedures to model the progressive mechanical degradation of the material under stress. This is illustrated by the numerical simulation of the mechanical behaviour of a clayey sand and a rock-type material.*

1 INTRODUCTION

Heterogeneous geomaterials possess complex microstructures. The main difficulties encountered in multi-scale modeling of geomaterials, at small scale, are related to the complexity of the geometry, the natural disorder and the variety of contributing multi-physical phenomena. The computational homogenisation of such microstructures requires specific tools to take this complexity into account, both from the point of view of the availability of representative volume elements, and from the point of view of the discretization technique. In this work, those two specific aspects are addressed through the development of generic tools for the generation of controlled microstructure, based on a topology-independent geometrical representation (level set) (Sethian, 1999) and a heterogeneity independent discretization methodology, consisting in a level set-based extended finite element description (XFEM) (Sukumar et al., 2001, Moes et al., 2003). A fine-scale plastic constitutive law is used to model the progressive mechanical degradation under mechanical loading. The scale transition to obtain the macroscopic stress-strain

relationship from the computation at micro-scale is obtained through a periodic homogenization scheme (Kouznetsova et al., 2001, 2002, Massart and Selvadurai, 2012).

2 PERIODIC HOMOGENEIZATION

Scale transition techniques are used to obtain the average (macroscopic) material properties of a homogeneous equivalent material based on microstructural descriptions including fine-scale heterogeneities and the constitutive laws of each phase. Consequently, the experimental parameter identification is transferred to lower scales on which phenomenologically simpler laws can be used.

The averaged mechanical properties of a heterogeneous material can be deduced by loading a Representative Volume Element (RVE) containing the main microstructural features of the material, and solving the corresponding equilibrium problem. When a macroscopic strain E is applied to a RVE, the displacement of a point inside the RVE is given by

$$\vec{u}(\vec{x}) = E.\vec{x} + \vec{u}_f(\vec{x}) \tag{1}$$

where $\vec{x}$ is the position vector within the RVE and $\vec{u}_f$ is a fluctuation field caused by the heterogeneity of the material. Assuming that the macroscopic strain is the volume average of the fine-scale strain field ε resulting from the above equation, and accounting for a periodic fluctuation, the Hill-Mandel condition (energy equivalence between the fine-scale and macroscopic descriptions)

$$\Sigma : \delta E = \frac{1}{V}\int_V \sigma : \delta\varepsilon \; dV \tag{2}$$

implies that the macroscopic stress tensor is obtained as the volume average of the microstructural stress tensor. Considering the periodicity of the fluctuation field, the macroscopic stress tensor can next be identified based on the cell tying forces at nodes controlling the macroscopic loading as

$$\Sigma = \frac{1}{V}\int_V \sigma \; dV = \frac{1}{V}\sum_{a=1}^{4} \vec{f}^{(a)}\vec{x}^{(a)} \tag{3}$$

where the summation spans the nodes controlling the RVE loading, $\vec{f}^{(a)}$ and $\vec{x}^{(a)}$ are, respectively, the nodal force and the nodal displacement of the node (a). The periodicity of the microfluctuation field can be enforced by homogeneous linear connections between corresponding faces. In a three-dimensional body, four controlling points (denoted 1 to 4 in Fig. 1) are used to apply the macroscopic stress or deformation modes of the boundary of the RVE, provided identical meshes are used on the opposite faces of the RVE.

The RVE equilibrium problem under the macroscopic stress loading is then solved by imposing forces $\vec{f}^{(a)}$ at the controlling points, which represent the action of the neighboring continuum on the RVE. The displacements of the controlling points, energetically conjugated to the imposed controlling forces, can be used to extract the macroscopic strain. A full description of the homogenization scheme can be found in Massart and Selvadurai (2012).

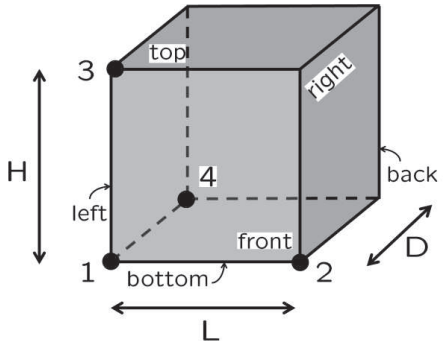

Fig 1. Control points for macroscopic quantities control on a RVE for upscaling principles

3 MICROSTRUCTURE GENERATION

The numerical modeling of the geomaterial behaviour at micro-scale requires, first, a proper representation of the microscopic morphology (at the particle scale). Two alternatives can be adopted to consider a representative microstructure: (i) the extraction of a real microstructure from the image analysis of full-field experimental methods of material observations (e.g. Computed X-Ray Tomography) (Hashemi et al., 2013) or (ii) the computed generation of microstructure respecting some constraints (e.g. prescribed volume fractions and/or grain size distributions) (Sonon et al., 2012). The main advantage of the second method is that representative microstructures can be randomly generated providing a large number of possible morphologies for a same set of constraints. Also, it does not require sophisticated techniques of sample observations.

In the present work, a specific methodology for the computed generation of microstructures has been developed. The RVE generator tool is mainly designed for granular media, possibly cemented, bridged or coated by a matrix material as well as polycrystalline media. It is based on distance fields and level set functions as presented in Sonon et al. (2012) for 2D RVEs, and extended in Sonon et al. (2013) for 3D simulations.

Three tools are combined to build an RVE starting from a random distribution of inclusions (inclusion packing, Section 3.1) that can be morphed (inclusion morphing, Section 3.2) to achieve specific features, and completed with a specific binding phase (Coating/bridging paste, Section 3.3).

3.1 Inclusion packing

The inclusion packing is the first step of the RVE generation method that gives the basis for the microstructural spatial arrangement. It allows incorporating prescribed volume fractions and grain size distributions as input parameters. The geometry used for the shape of inclusions is arbitrary and can be randomly generated through a parameterization or explicitly defined from existing data (e.g. in order to use data from Computed X-Ray Tomography).

The problem of filling a container with a given volume fraction of inclusions while respecting prescribed size distributions and grain shapes is achieved here using a Random Sequential Addition (RSA) of inclusions (Cooper, 1988), improved by the use of distance fields. The method is called LS-RSA (for Level-Set controlled Random Sequential Addition, Sonon et al. (2012)). With this original method, the efficiency of the sequential addition of inclusion is drastically improved using distance fields. Instead of a purely random trial position, a set of discrete positions satisfying a priori the non-overlapping and neighboring distance conditions is used to select new inclusion locations. Consequently, trial positions are

never rejected, as it is often the case for the classical RSA algorithm (mainly when dense packing must be reached).

The available zone for the addition of the next inclusion is built using the nearest neighbor distance function $LS_1(\vec{x})$ (see Fig. 2a) which is maintained on a structured grid of points $\vec{x}_n$ at each inclusion addition. The radius r of the smallest enclosing circle (or sphere) of the new inclusion is used as an indicator of its size. The positions on the grid leading to overlap with existing inclusions can be excluded for the random inclusion positions by allowing selection only among the points of the grid satisfying the condition (Fig.2a)

$$LS_1(\vec{x}_n) > r \tag{4}$$

This allows the addition of a new inclusion at each trial, and the generation cost is therefore not linked to any probability relative to the actual density, but rather to the number of added inclusions. Additional neighboring distance conditions can be enforced using $LS_1(\vec{x})$ such as for instance

$$nn_{\min} + r < LS_1(\vec{x}_n) < nn_{\max} + r \tag{5}$$

where $nn_{\min}$ and $nn_{\max}$ are the minimum and maximum distance imposed from the first neighbor of the added inclusion (Fig. 2a). To increase packing density, the spatial organization has to be optimized by minimizing the distances of the added inclusion to its second nearest neighbor in 2D and its third nearest neighbors in 3D. The corresponding distance functions $LS_2(\vec{x})$ and $LS_3(\vec{x})$ are used for this purpose with the same type of condition (Fig. 2b).

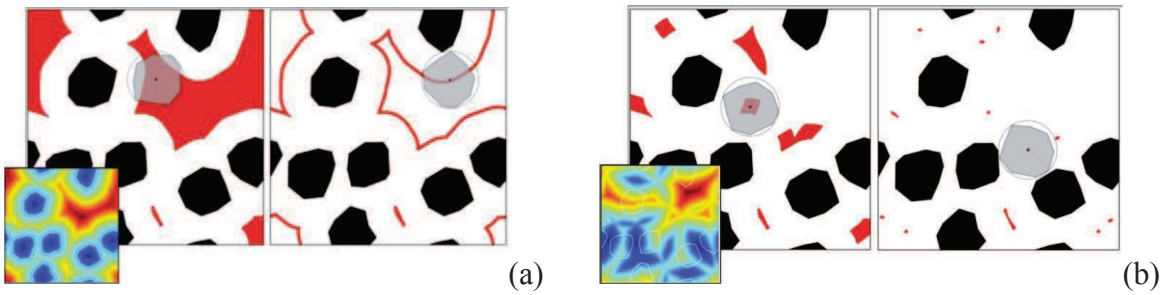

Fig 2. (a) Non-overlap and first neighbor distance criteria to restrict the random position of the new inclusion to be added (the function $LS_1(\vec{x})$ is represented in the insert), (b) First and second neighbor distance criteria to optimize spatial organization to obtain dense packing (the function $LS_2(\vec{x})$ is represented in the insert)

3.2 Inclusion morphing

Marginal corrections required to adjust the inclusion volume fraction or shapes and more substantial modifications allowing to produce polycrystalline or cellular microstructures motivate the development of a tool enabling the morphing of inclusions once their population is entirely generated by sequential addition. At this stage, the inclusions neighborhood is completely determined and can be used to modify their shape according to inter-inclusion distance rules. A complete expansion of inclusions until vanishing of the inter-grain joint thickness allows forming polycrystal-like microstructures.

The morphing technique is strongly based on level set functions. The $LS_1(\vec{x}_n)$ and $LS_2(\vec{x}_n)$ functions built during the sequential addition process are used to construct a function $O(\vec{x}_n)$ that can be contoured to extract updated shapes of the inclusions. The function

$$O(\vec{x}_n) = LS_1(\vec{x}_n) - LS_2(\vec{x}_n) \tag{6}$$

vanishes at points of equal distance between two nearest inclusions and is negative elsewhere. The zero level set of this function thus determines a Voronoï-like diagram, each cell enclosing an inclusion and points closer to it than to other inclusions. If the initial inclusion distribution is a dense arrangement of mono-sized spheres, the produced grains are convex and the result is exactly a Voronoï diagram (Fig. 3a). The use of multi-sized arbitrary shaped polyhedra leads to disordered microstructures (Fig. 3b). A joint between the grains with constant thickness w can be obtained by considering the function $O(\vec{x}_n) = LS_1(\vec{x}_n) - LS_2(\vec{x}_n) + w$.

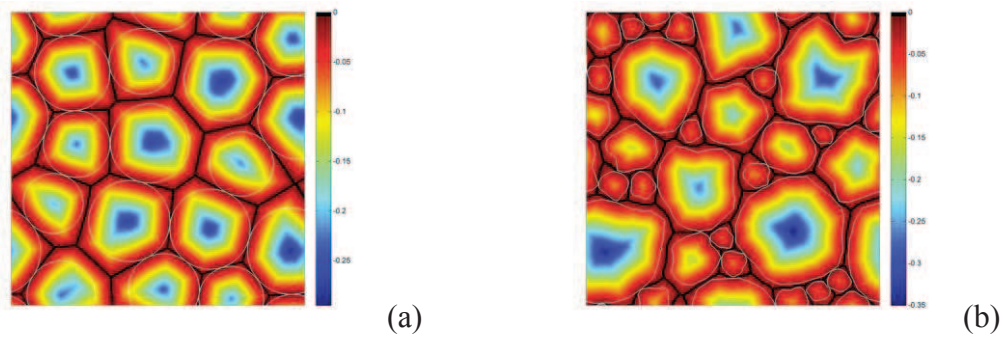

(a) (b)

Fig 3. (a) Convex Voronoï-like cells produced by a mono-sized spheres packing, (b) disordered cells produced by an arbitrary shaped multi-sized inclusion packing

3.3 Coating/bridging paste

The presented methodology also allows generating coatings and bridges around inclusions. It may reproduce, for instance, the clayey bridge between coarse particles of sand in clayey sand. Cement paste of concretes or precipitate coating in cemented rocks are others examples that can correspond to this coating paste.

On the one hand, a uniform coating of thickness w is trivially extracted with the w level set of $LS_1(\vec{x})$. On the other hand, bridges between two neighboring inclusions can be generated provided the inter-distance between two potentially bridged grains is small enough. The function $O(\vec{x}_n) = LS_1(\vec{x}_n) - LS_2(\vec{x}_n)$ (Fig.4) contains explicitly in each point n the distance between the two nearest point via n. The zero level set of $O(\vec{x}_n) = LS_1(\vec{x}_n) - LS_2(\vec{x}_n) - b$ give the geometry of bridges linking grains closer to each other than b.

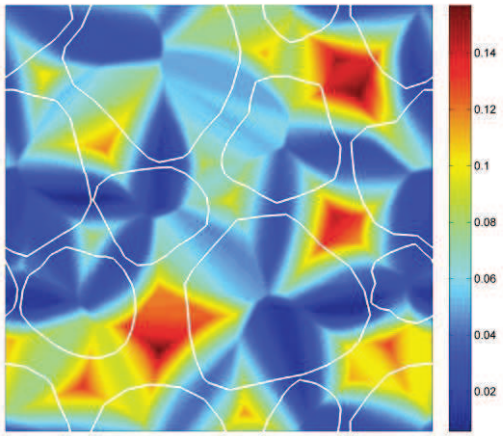

Fig 4. The function $O(\vec{x}_n) = LS_1(\vec{x}_n) - LS_2(\vec{x}_n)$ explicitly contains the information to create bridging past between inclusions.

4 MECHANICAL MODEL

4.1 X-FEM Computation

The complexity of generating finite element meshes for the generated RVEs motivates the use of an alternative discretization method. The eXtended Finite Element Method (Sukumar et al., 2001, Moës et al., 2003), that does not require meshes conforming to the material boundaries, is therefore used. In addition to be defined as an extension of the standard finite element scheme, this method uses the level set formalism to describe the RVE geometry, which allows its seamless integration with the RVE generator.

The principle of XFEM is to use a non-conforming regular mesh with additional degrees of freedom related to additional shape functions (denoted the enrichment) introducing the strain jumps induced by material heterogeneities. This treatment, concentrated on finite elements intersected by a material interface (e.g. inclusion/matrix boundary), uses signed distance functions to construct the enrichment and to subdivide elements by material at the stiffness integration stage. The interpolation of each displacement field components therefore reads

$$u_{XFEM}(x) = \sum_i N_i(x) d_i + \sum_i N_j(x) \Psi(x) a_j \tag{7}$$

where the first term represents the usual finite element polynomial interpolation containing the standard shape functions as a partition of unity. The second term introduces the XFEM enrichment with a_j the additional unknowns and $\Psi(x)$ the enrichment functions. For heterogeneous materials, the LS_1 level set (distance) function was shown to introduce the required strain jump at the material boundary. The XFEM methodology implemented in a 3D setting is coupled with periodic homogenization and fully compatible with the RVEs generated using the tools presented previously.

4.2 Elasto-plastic constitutive model

The elastic part of the deformation is considered through classical linear elasticity including constant values of the Young modulus and the Poisson ratio. The limit between the elastic and the plastic domain is represented by a Drucker-Prager yield surface:

$$f \equiv q - Mp - k = 0 \quad \text{with} \quad M = \frac{6\sin\phi}{3-\sin\phi} \quad \text{and} \quad k = \frac{6c\cos\phi}{3-\sin\phi} \tag{8}$$

where p and q are the mean stress and the deviatoric stress and c and ϕ are the cohesion and the friction angle, respectively. An associate flow rule is considered producing dilatancy upon plastic shearing (the dilatancy angle is equal to friction angle):

$$\dot{\varepsilon}_{ij}^{p} = \dot{\lambda}^{P} \frac{\partial f}{\partial \sigma_{ij}} \tag{9}$$

Progressive hardening is introduced through the evolution of the cohesive term with the deviatoric strain (corresponding to the plastic multiplier $\dot{\lambda}^{P}$):

$$k = k_0 + A\,\dot{\lambda}^{P} \tag{10}$$

5 RESULTS

5.1 Clayey sand

In this section, we deduce the macroscopic behaviour of a lime-treated clayey sand through the consideration of its mechanical behaviour at micro-scale. To achieve this, a representative microstructure was generated through the microstructure generation tool detailed in Section 3. Periodic conditions have been applied on the boundaries of the RVE. Then, the mechanical problem has been addressed through the XFEM scheme considering a linear elastic response of the sand grains and elasto-plastic behaviour of the clay matrix. Material parameters are reported in Table 1. The inclusion packing generates the inert grain (considered >2μm) in agreement with the grain size distribution of inert particles. A bridging paste is introduced to represent the clayey matrix corresponding to the soil particles <2μm. This distinct phase contains the clay particles, a certain quantity of lime from the treatment and micro-voids including water and air. This phase plays an important cohesive role, acting as a matrix, coating and bridging inert grains together.

This framework allows modeling, observing and understanding the basic mechanisms of plasticity propagation in the microstructure as well as studying the evolution of macroscopic elastic limit as a function of the morphology. A first application, assuming a 2D plane-strain problem, compares the macroscopic response of two specimens containing two different clay contents under oedometric compression (application of vertical loading while macroscopic radial displacements are constrained). Results are depicted in Figure 5. It is shown that even if the macroscopic stress state is mainly isotropic (with a low deviatoric component compared to the mean stress), the local microstructure contains many zones in which deviatoric strains occur. This is particularly the case in the clayey bridging zones where the distance between two sand particles is small. The specimen with the lower clay content exhibits the softer response and the lower elastic limit. This may seem counterintuitive because clay is the

compressible phase in the medium. However, this feature of behaviour has also been observed experimentally. Until a certain quantity, clay has a positive effect on the stiffness and strength of clayey sand. Clay reinforces the particles contacts, provides cohesion and avoids strain localization in the particle contacts.

The microstructure of a soil is highly three-dimensional and there is no trivial way to find a 2D mechanically equivalent description of a given 3D sample. Some morphological aspects concerning voids topology only emerge in 3D and the number of kinematically admissible mechanisms is also different. There is also no comparison possible in terms of volume fractions. Consequently, the clayey sand application is generalized in 3D with a clay content of 30 %. The same methodology is applied. However, up to now, due to computation time constraints, plasticity was not considered and a purely elastic computation is performed. Even if the behaviour of the clay matrix is not perfectly representative of real plastic clay, some general trends can be observed in terms of strain distribution in the microstructure (Figure 6). Strains are concentrated in the short clay bridges. The largest grains carry the main part of the stress. Chain forces are mainly developed across those large grains. Consequently, the largest strains occur mainly in the clayey bridges surrounding largest sand grains (see Figure 6, right).

Table 1. Material parameters used in the different mechanical computations

Materials	E [GPa]	υ [-]	c [MPa]	ϕ [°]	A [GPa]
Clayey sand 2D					
Sand particles	10	0.1	-	-	-
Treated clay matrix	0.5	0.2	0.5	23°	Perfectly plastic
Clayey sand 3D					
Sand particles	10	0.1	-	-	-
Treated clay matrix	0.5	0.2	-	-	-
Rock-type material					
Grains	60	0.1	-	-	-
Joints	30	0.3	40	17	1

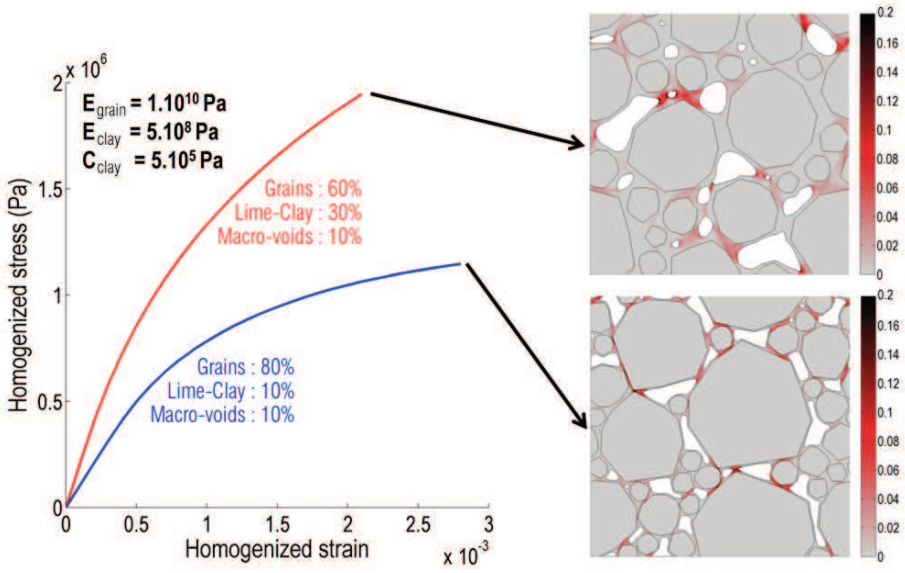

Fig 5. Macroscopic behaviour of lime-treated clayey sand upon oedometric compression interpreted from micro-scale computations. Focus on the effect of the clay content. The snapshots on the right represent the distribution of vertical strain in the microstructure. The size of RVE is 10 mm along each direction.

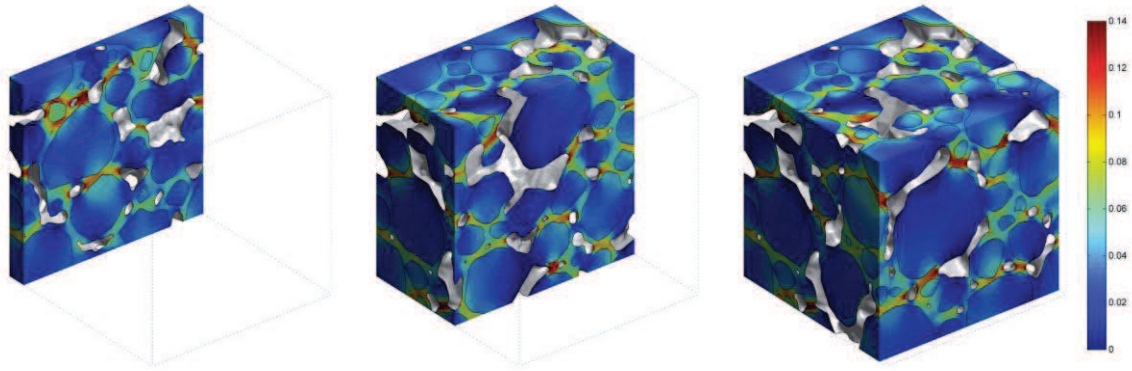

Fig 6. Vertical strain distribution obtained from 3D elastic computation of lime-treated clayey sand upon oedometric compression. The size of RVE is 10 mm along each direction.

5.2 Rock-type material

As opposed to soil-type materials, rock-type materials do not exhibit macro-voids and the material can be considered as a continuum medium, even at micro-scale. The existing voids are included in the rock matrix. A 3D microstructure made of grains and large joints with a grain volume fraction of 58% was generated with the LS-RSA tool (Figure 7) and subjected to triaxial loading. The grains do not present any preferential orientation. They are assumed purely elastic, whereas a plastic behaviour is assumed in the joints. The set of parameters used in the computations is defined in Table 1. The applied loading follows a typical triaxial test with a strong confinement. A confinement of 100 MPa is first applied in all directions, followed by an increase of the axial stress, the other stress components remaining fixed. This high confining stress is used to avoid any convergence problem in the mechanical problem, and to keep the local strain distribution consistent with a small strain description. The strain are still concentrated in the weakest phase (the joints) while the grains remain almost unstrained. The plastic dilatancy in the joints produces high dilatant volumetric strains. The macroscopic mechanical response of the RVE is depicted in Figure 8.

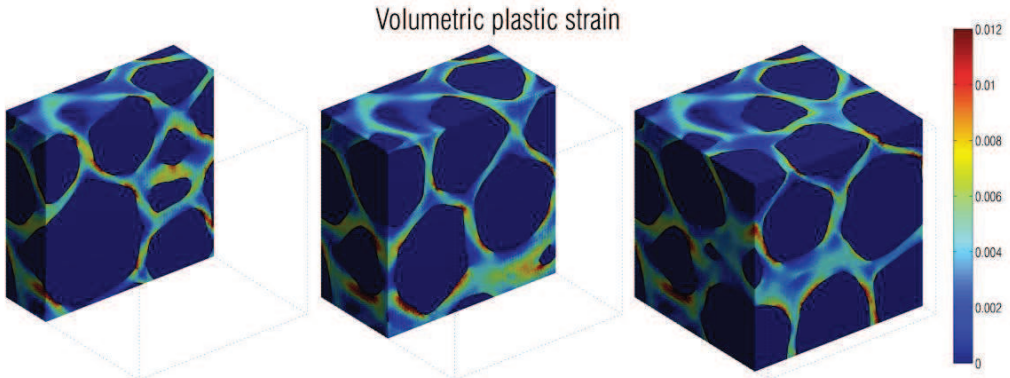

Fig 7. Volumetric strain distribution obtained in the rock-type material at 350 MPa of deviatoric stress. Strains occur in the joints. The size of RVE is 10 mm along each direction.

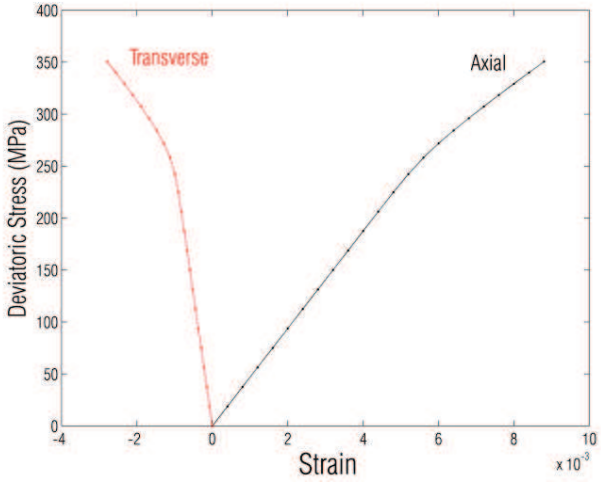

Fig 8. Homogenized response of the RVE. Mechanical response under triaxial conditions depicting the average deviatoric stress applied as a function of the axial and transverse strains.

6 CONCLUSIONS

An efficient methodology including microstructural RVE generation of porous media combined with a XFEM computational scheme has been proposed to investigate the mechanical properties of heterogeneous geomaterials at small scale. A periodic homogenization scheme allows the scale transition in order to deduce homogenized response of the material from a macroscopic point of view. This framework allows understanding the basic mechanisms of plasticity propagation which control the mechanical response at macroscopic (laboratory) scale. In companion works (Massart and Selvadurai, 2012, Sonon et al., 2013), the obtained local damage propagation from the mechanical computations is coupled with fluid transport modeling, which allows identifying microstructural features responsible for permeability evolution due to mechanical degradation.

ACKNOWLEDGEMENT

The first author gratefully acknowledges F.R.S-FNRS Belgium for funding through the FRIA grant 5.0.011.12.F.

REFERENCES

Cooper D.W. (1988). Random-sequential-packing simulations in three dimensions for spheres, Phys. Rev. A 38, 522–524.

Hashemi M.A., Khaddour G., François B., Massart T.J., Salager S. (2013). A tomographic imagery segmentation methodology for multi-phase granular materials based on simultaneous region growing. Submitted.

Kousnetsova V., Brekelmans W.A.M., Baaijens F.T.P. (2001). An approach to micro–macro modeling of heterogeneous materials, Comput. Mech. 27, 37–48.

Kouznetsova V., Geers M.G.D., Brekelmans W.A.M. (2002). Multi-scale constitutive modelling of heterogeneous materials with a gradient-enhanced computational homogenization scheme, Int. J. Numer. Methods Engrg. 54, 1235–1260.

Massart T.J., Selvadurai A.P.S. (2012). Stress-induced permeability evolution in a quasi-brittle geomaterial, J. Geophys. Res., 117 B07207.

Moes N., Cloirec M., Cartraud P., Remacle J.F. (2003). A computational approach to handle complex microstructure geometries, Comp. Meth. Appl. Mech. Engng. 192(28-30), 3163-3177.

Sethian J.A. (1999). Level Set Methods and Fast Marching Methods, Cambridge University Press, New York.

Sonon B., François B., Massart T.J. (2012). A unified level set based methodology for fast generation of complex microstructural multi-phase RVEs, Comp. Meth. Appl. Mech. Engng. 223-224, 103-122.

Sonon B., François B., Massart T.J. (2013). Generation of complex three-dimensional RVEs for computational homogenisation, In preparation.

Sonon B., François B., Selvadurai A.P.S., Massart T.J. (2013). XFEM modelling of degradation-permeability coupling in complex geomaterials. 13th International Conference on Fracture.

Sukumar N., Chopp D.L., Moës N., Belytschko T. (2001). Modeling holes and inclusions by level sets in the extended finite-element method. Comput. Methods Appl. Mech. Engrg. 190, 6183–6200.